Hybrid quantum-classical method for simulating high-temperature dynamics of nuclear spins in solids

Grigory A. Starkov[1,2,*] and Boris V. Fine[1,3,†]

[1]*Skolkovo Institute of Science and Technology, Skolkovo Innovation Centre, Nobel Street 3, Moscow 143026, Russia*
[2]*Lebedev Physical Institute of the Russian Academy of Sciences, Leninsky prospect 53, Moscow 119991, Russia*
[3]*Institute for Theoretical Physics, University of Heidelberg, Philosophenweg 12, 69120 Heidelberg, Germany*

(Received 3 July 2018; revised manuscript received 26 October 2018; published 12 December 2018)

First-principles calculations of high-temperature spin dynamics in solids in the context of nuclear magnetic resonance (NMR) are a long-standing problem, whose conclusive solution can significantly advance the applications of NMR as a diagnostic tool for material properties. In this work, we propose a hybrid quantum-classical method for computing NMR free induction decay(FID) for spin-1/2 lattices. The method is based on the simulations of a finite cluster of spins 1/2 coupled to an environment of interacting classical spins via a correlation-preserving scheme. Such simulations are shown to lead to accurate FID predictions for one-, two-, and three-dimensional lattices with a broad variety of interactions. The accuracy of these predictions can be efficiently estimated by varying the size of quantum clusters used in the simulations.

DOI: 10.1103/PhysRevB.98.214421

I. INTRODUCTION

Free induction decay (FID) measured by nuclear magnetic resonance (NMR) is, normally, proportional to the infinite-temperature time autocorrelation function of the total nuclear spin polarization of the system [1,2]. It depends on the internuclear distances and spin-spin interactions. The Fourier transform of the FID gives the NMR absorption line shape [1–3]. First-principles calculation of NMR FID in solids is a nonperturbative problem—it does not have a small parameter to build a controllable analytic expansion. The problem is normally nonintegrable at the quantum level [4] and chaotic at the classical level [5,6]. It belongs to a broader class of problems exhibiting non-Markovian dynamics, often accompanied by nonuniversal observable behavior. A number of first-principles methods of FID calculations have been proposed in the past [1,2,7–19]. Quite a few of them produced good approximations for FID in one system, namely, CaF_2 [1,20]. Yet none of them is widely used at present because their predictive performance for a broader class of systems is either poor or unclear. In the present work, we propose a hybrid quantum-classical method of simulating high-temperature spin dynamics that meets the challenge of predictive performance in two ways: the method is tested for one-, two-, and three-dimensional spin-1/2 lattices with a broad variety of interactions, and simultaneously, it is shown that one can make an efficient uncertainty estimate for the computed quantity. The defining feature of the method is the implementation of the dynamical action of the quantum cluster on the classical environment.

The method of hybrid simulations is likely to be applicable beyond solid-state NMR to describe, for example, quantum decoherence [17,21–25] and inelastic magnetic neutron scattering at high temperatures [26]. The advantage of developing the method in the context of NMR is the availability of a very accurate experimental testing ground, which is a consequence of the fact that nuclear spin dynamics is well isolated from the electronic and phononic environments.

II. MODEL

We consider a lattice of spins 1/2 with a translationally invariant Hamiltonian of the general form

$$\mathcal{H} = \sum_{\alpha, i<j} J^{\alpha}_{i,j} S^{\alpha}_i S^{\alpha}_j, \qquad \alpha \in \{x, y, z\}, \tag{1}$$

where S^{α}_i is the operator of spin projection on axis α for the ith lattice site and $J^{\alpha}_{i,j}$ are the coupling constants. The quantities of our interest are time autocorrelation functions of the total spin polarization $M_\alpha = \sum_i S^{\alpha}_i$,

$$C_\alpha(t) = \langle M_\alpha(t) M_\alpha(0)\rangle / \langle M^2_\alpha\rangle, \tag{2}$$

where $\langle \cdots \rangle$ denotes the averaging over the infinite-temperature equilibrium state. In general, $C_\alpha(t)$ decays on the fastest microscopic timescale of the system characterized by the inverse rms value of local fields experienced by each spin:

$$\tau_c = \left(\sum_j J^{x\,2}_{ij} \langle S^{x\,2}_j\rangle + J^{y\,2}_{ij} \langle S^{y\,2}_j\rangle + J^{z\,2}_{ij} \langle S^{z\,2}_j\rangle \right)^{-1/2}. \tag{3}$$

Direct numerical calculation of $C_\alpha(t)$ in the thermodynamic limit is not feasible due to the exponentially large Hilbert spaces involved.

III. HYBRID METHOD

We replace the above quantum lattice with a hybrid lattice that contains a set of lattice sites $\mathcal{Q}$ occupied by a cluster of

*grigory.starkov@skolkovotech.ru
†b.fine@skoltech.ru

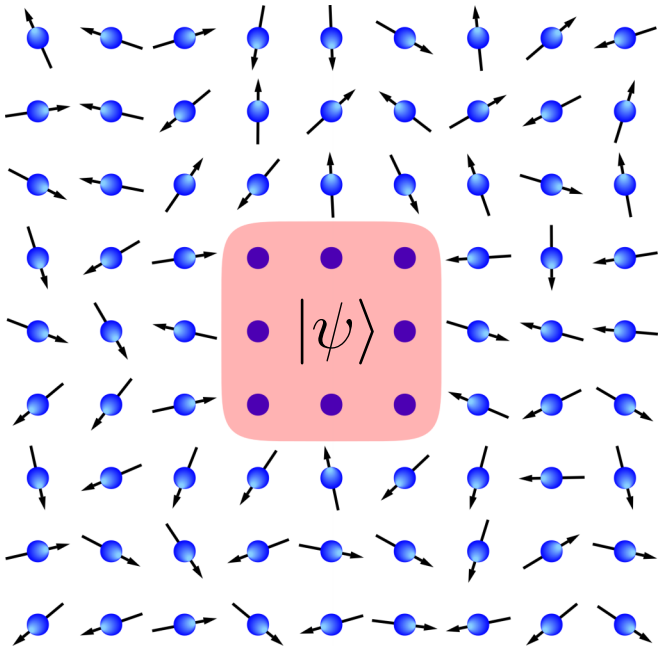

FIG. 1. Sketch of a hybrid lattice: a cluster of spins 1/2 surrounded by an environment of classical spins. The quantum cluster is described by a wave function $|\psi\rangle$. Classical spins are represented by three-dimensional vectors.

quantum spins 1/2 and a set of sites $\mathcal{C}$ occupied by classical spins (see Fig. 1). The quantum cluster is described by a wave function $|\psi\rangle$, while the classical spins are described by a set of vectors $\{\mathbf{s}_m\}$. The time evolution of $|\psi\rangle$ is computed quantum mechanically by direct integration of the Schrödinger equation, and simultaneously, the dynamics of the classical spin vectors $\{\mathbf{s}_m\}$ is obtained by the integration of the classical equations of motion (see Appendixes A, B, and C). In the above formalism, the statistical behavior of the quantum cluster is characterized by averaging over many pure states. In other contexts, such an approach often exploits quantum typicality [27–32], which is the property of a single many-body pure state to accurately represent certain kinds of statistical averages. In the present context, however, we do not benefit from quantum typicality—the method requires actual averaging of quantum-mechanical expectation values over many pure states.

The challenge in defining the dynamics of a hybrid system is to reproduce dynamical correlations of the original fully quantum lattice as closely as possible. An important aspect of these correlations is the retarded action of each spin on itself and remote spins via interacting neighbors. In order to induce such correlations across the quantum-classical border, we introduce effective local fields exerted by the two parts on each other. The local fields exerted by the classical environment on quantum spins can be defined to have the standard form used in purely classical simulations. In order to define the reverse action of the quantum spins on the classical neighbors, one can try to take the expressions for the classical local fields and, in those expressions, replace classical spin projections s_m^α with the expectation values of quantum spin operators $\langle\psi|S_m^\alpha|\psi\rangle$. However, the problem with such an approach is that, for a typical pure state describing a cluster of $N_\mathcal{Q}$ spins 1/2, the expectation values $\langle\psi|S_m^\alpha|\psi\rangle$ are exponentially small [28,32,33]—they are suppressed by the factor $1/\sqrt{N+1}$, where $N = 2^{N_\mathcal{Q}}$ is the cluster's Hilbert space dimension (see Appendix D for the derivation). Therefore, for $N \gg 1$, such a naive approach would lead to a negligible action of quantum spins on the classical ones, thereby failing to induce qualitatively important correlations across the quantum-classical border. Instead, we propose to use the quantum expectation values scaled up by the factor $\sqrt{N+1}$, whenever they are coupled to or combined with the classical variables. This rescaling will be justified after we introduce the formalism. Everywhere below, we further assume that $N \gg 1$ and hence replace the scaling factor $\sqrt{N+1}$ by $\sqrt{N}$.

The dynamics of the quantum and classical parts are described by the respective Hamiltonians

$$\mathcal{H}_\mathcal{Q} = \sum_{i<j,\alpha}^{i,j\in\mathcal{Q}} J_{i,j}^\alpha S_i^\alpha S_i^\alpha - \sum_{i\in\mathcal{Q}} \mathbf{h}_i^{\mathcal{CQ}} \cdot \mathbf{S}_i, \tag{4}$$

$$\mathcal{H}_\mathcal{C} = \sum_{m<n,\alpha}^{m,n\in\mathcal{C}} J_{m,n}^\alpha s_m^\alpha s_n^\alpha - \sum_{m\in\mathcal{C}} \mathbf{h}_m^{\mathcal{QC}} \cdot \mathbf{s}_m, \tag{5}$$

where S_i^α are the operators of spins 1/2 as in Eq. (1), $\mathbf{s}_m \equiv (s_m^x, s_m^y, s_m^z)$ are vectors of length $\sqrt{S(S+1)} = \sqrt{3}/2$ representing classical spins, and $\mathbf{h}_i^{\mathcal{CQ}}$ and $\mathbf{h}_i^{\mathcal{QC}}$ are the local fields coupling the quantum and the classical parts:

$$\mathbf{h}_i^{\mathcal{CQ}} = -\sum_{n\in\mathcal{C}} \begin{pmatrix} J_{i,n}^x s_n^x \\ J_{i,n}^y s_n^y \\ J_{i,n}^z s_n^z \end{pmatrix}, \tag{6}$$

$$\mathbf{h}_m^{\mathcal{QC}} = -\sqrt{N} \sum_{j\in\mathcal{Q}} \begin{pmatrix} J_{m,j}^x \langle\psi|S_j^x|\psi\rangle \\ J_{m,j}^y \langle\psi|S_j^y|\psi\rangle \\ J_{m,j}^z \langle\psi|S_j^z|\psi\rangle \end{pmatrix}. \tag{7}$$

The lattice has periodic boundary conditions.

The initial conditions for the simulations include a fully random choice of $|\psi(0)\rangle$ in the Hilbert space of the quantum cluster and random orientations of classical spins. The hybrid version of the total spin polarization $M_\alpha(t)$ is defined according to the earlier prescription for rescaling quantum expectation values:

$$M_\alpha(t) = \sqrt{N}\langle\psi(t)| \sum_{i\in\mathcal{Q}} S_i^\alpha |\psi(t)\rangle + \sum_{m\in\mathcal{C}} s_m^\alpha(t). \tag{8}$$

The mathematical construction based on Eqs. (4), (5), (6), (7), and (8) introduces dynamical correlations across the quantum-classical boundary, which, while being approximate, exactly capture two important aspects of the fully quantum dynamics. First, the rms value of the local field for each spin, quantum or classical, is the same as that for the original quantum lattice. Second, if the Hamiltonian of the original quantum lattice conserves the total spin polarization or one of its projections, this conservation law is also respected by the hybrid dynamics for M_α defined by Eq. (8).

Yet the quantum-classical border still disturbs the dynamics of spins within the quantum cluster in comparison with the purely quantum lattice. This distortion is weaker for the spins

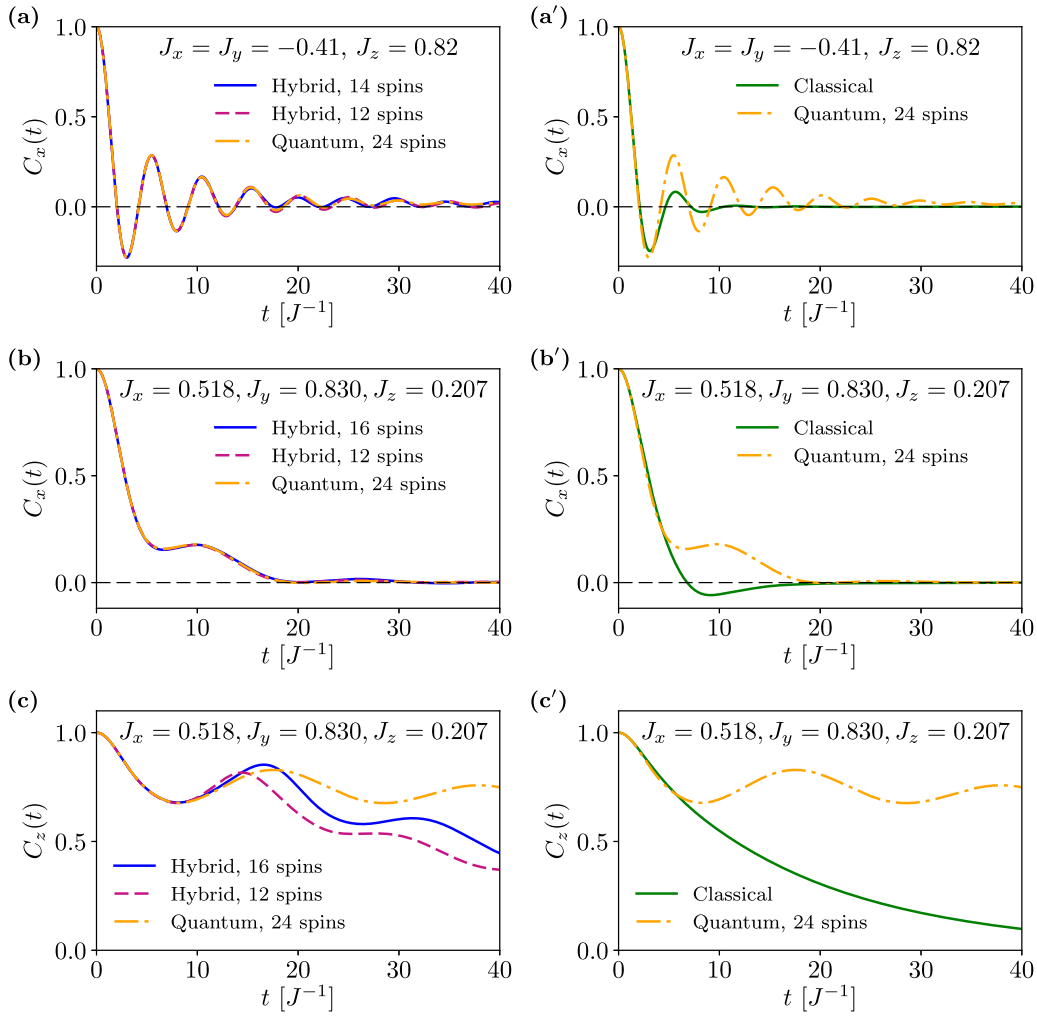

FIG. 2. Correlation functions $C_\alpha(t)$ for one-dimensional periodic chains with nearest-neighbor interactions. The interaction constants are indicated above each plot. The left column compares the results of hybrid simulations with the reference plots obtained by direct quantum calculations. The right column does the same for purely classical simulations. For both hybrid and classical simulations, the full lattice size is 92. The sizes of quantum clusters in hybrid simulations and in reference quantum calculations are indicated in the legends.

located farther from the border. Therefore, as explained in Appendix E, we reduce the influence of the border by introducing an auxiliary variable $M'_\alpha = \sqrt{N}\langle\psi(t)|\sum_{m\in\mathcal{Q}'} S^\alpha_m|\psi(t)\rangle$, where the subset $\mathcal{Q}'$ is limited to one or several central spins within the quantum cluster. We then compute the correlation function of interest as

$$C_\alpha(t) = \langle M_\alpha(t) M'_\alpha(0)\rangle / \langle M'^2_\alpha\rangle \tag{9}$$

by performing averaging over the equilibrium noise of $M_\alpha(t)$ and $M'_\alpha(t)$.

An important aspect of the hybrid method is that it is possible to make an efficient estimate of the accuracy of its predictions. This estimate is based on the observation that, as the size of the quantum cluster increases, the hybrid calculation must converge to the exact quantum result. Therefore, a discrepancy between the results for quantum clusters of significantly different sizes gives an estimate of the difference with the thermodynamic limit. The implementation of the hybrid method can realistically involve only relatively small quantum clusters of 10–20 spins 1/2. Yet, precisely for this reason, the relative differences between these sizes are large. Therefore, if these differences do not lead to large deviations of the computed correlation functions, then the result should be viewed as reliable. For lattices with a not too small number of interacting neighbors, where purely classical calculations are expected to work well [19], the deviation between a purely classical calculation and a hybrid calculation with a small quantum cluster can already be sufficient for a reasonable estimate of the predictive accuracy. (See also the remark at the end of Appendix D.)

IV. TESTS OF THE HYBRID METHOD

A. Comparison with direct numerical simulations

Our tests of the performance of the hybrid method for one-dimensional chains and two-dimensional square lattices of spins 1/2 are presented in Figs. 2 and 3, respectively. The lattices had nearest-neighbor interactions with coupling constants indicated in the legends. In both figures, the predictions of the hybrid method are compared with the results of numerically exact direct quantum simulations for sufficiently large clusters. The cluster was considered "sufficiently large"

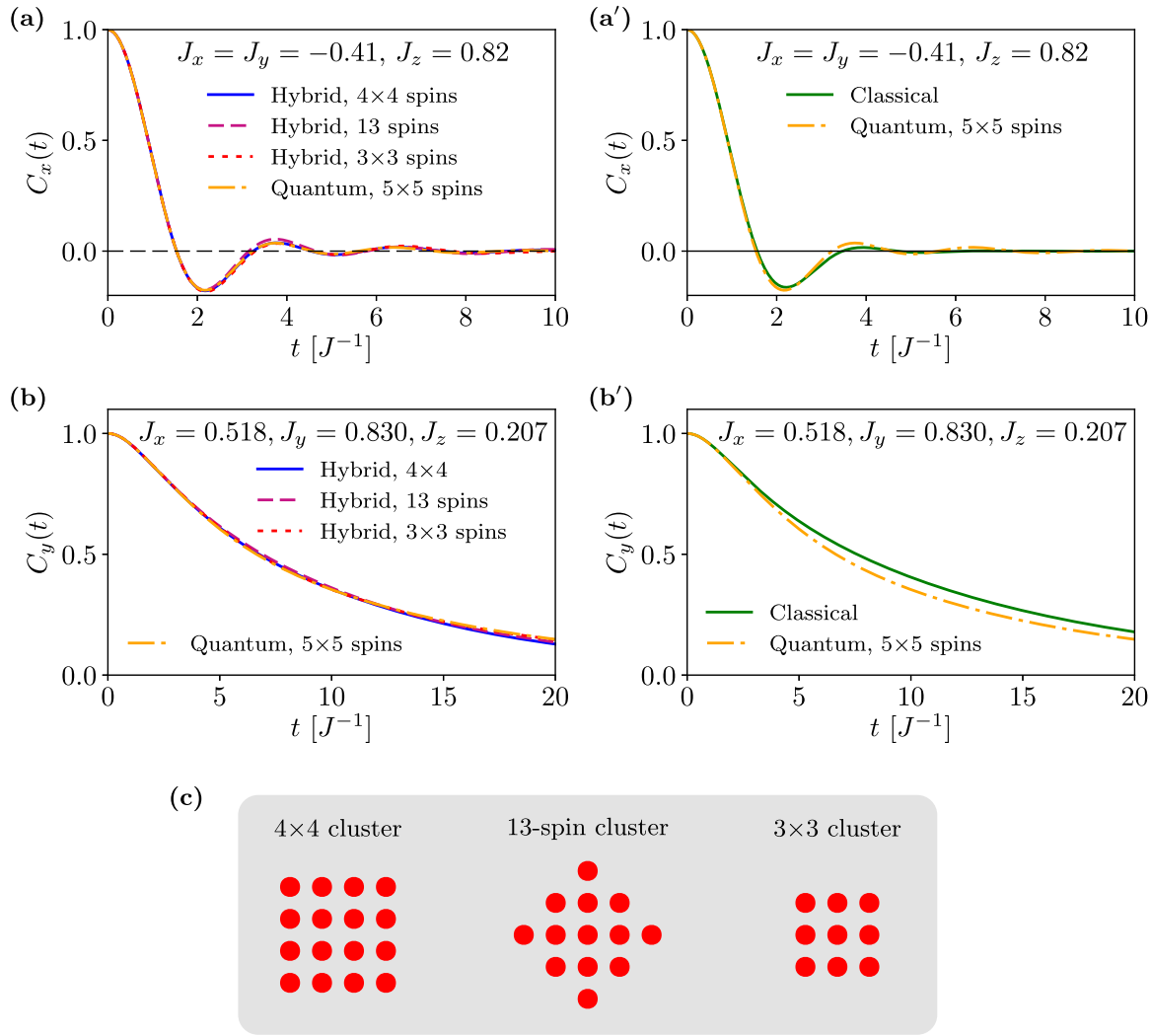

FIG. 3. Correlation functions $C_\alpha(t)$ for two-dimensional periodic lattices with nearest-neighbor interaction. The notations in (a)–(b′) are the same as in Fig. 2. For both hybrid and classical simulations, the full lattice size is 9×9. The shapes of quantum clusters for hybrid simulations are shown in (c).

when, in the time range of interest, the change in $C_\alpha(t)$ with the increase in the cluster size was negligible. The sizes of the quantum clusters for hybrid simulations were, typically, smaller: in comparison with direct simulations, they were limited by the requirement to generate many more and much longer quantum evolutions in order to collect enough statistics (see Appendix C). Figures 2 and 3 also include a side-by-side comparison of hybrid simulations with purely classical simulations. More such tests can be found in the Supplemental Material [34].

For one-dimensional chains, the performance of the hybrid simulations in Figs. 2(a) and 2(b) is excellent. These plots correspond to typical situations when correlation functions $C_\alpha(t)$ decay not too slowly, i.e., on a timescale of the order of τ_c. On the contrary, Fig. 2(c) illustrates an atypical case, where the coupling constants and the axis α are chosen such that $C_\alpha(t)$ decays anomalously slowly. In this case, the hybrid method's prediction exhibits a clear discrepancy from the reference plot. However, it is important to note the fact, illustrated in Fig. 2(c), that the internal estimate of the predictive accuracy based on the use of different quantum clusters within the hybrid method would anticipate the above discrepancy. We further note here that the same accuracy estimate in Figs. 2(a) and 2(b) is consistent with the observed excellent agreement with the reference plots. We, finally, observe that, in all cases presented in Fig. 2, the performance of the hybrid simulations is significantly better than that of the classical ones.

Figure 3 illustrates that, for two-dimensional lattices, hybrid simulations generally exhibit a very good performance, which is also noticeably better than that of the classical simulations, even though the latter is also reasonable, a consequence of the fact that the number of interacting neighbors of each spin has increased in comparison with the one-dimensional case [19].

B. Comparison with experiments

For three-dimensional lattices, direct numerical calculation of reliable reference plots for sufficiently large quantum clusters is not feasible. Therefore, we test the hybrid method by comparing its predictions with the NMR FID experiments [20] for ^{19}F nuclei in the benchmark material

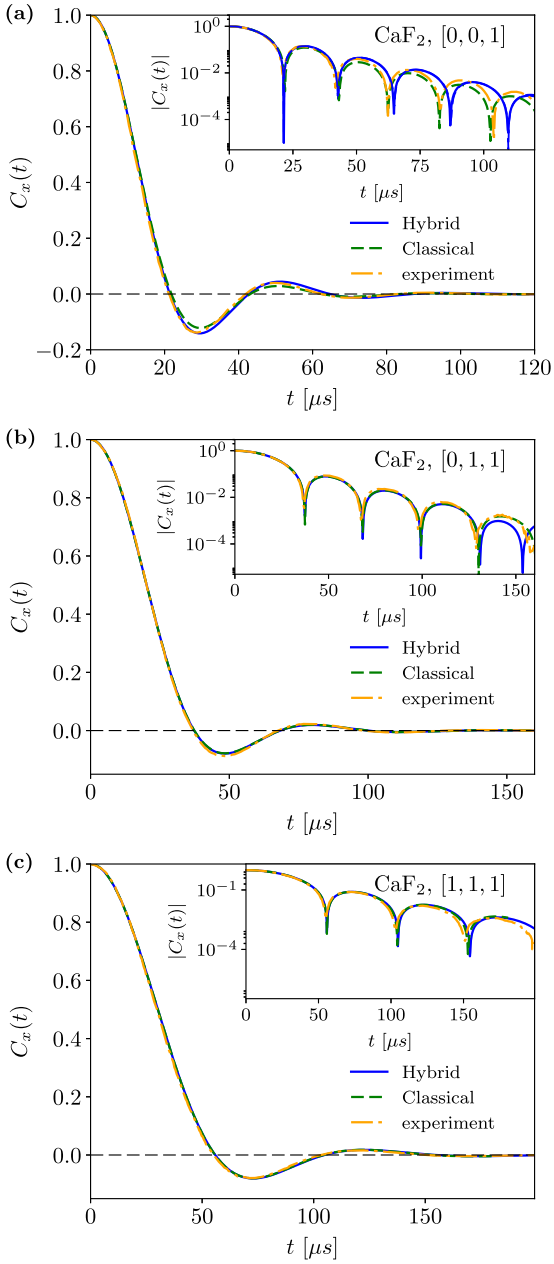

FIG. 4. FIDs in CaF_2 for external magnetic field B_0 along the following crystal directions: (a) [001], (b) [011], and (c) [111]. Hybrid and classical simulations are compared with the experimental results of Ref. [20]. For both hybrid and classical simulations, the full lattice size is $9 \times 9 \times 9$. The quantum cluster in hybrid simulations was a chain extending along the [001] crystal direction in (a), a chain passing through the entire lattice and oriented along the [100] crystal direction in (b), and a chain along the [111] crystal direction in (c). The insets contain semilogarithmic plots of the respective FIDs.

CaF_2. These nuclei have spin 1/2, form a cubic lattice, and interact via truncated magnetic-dipolar interaction (see Appendix F). In Fig. 4, we present a comparison between the experiment and the results of the hybrid and classical simulations for magnetic field $\mathbf{B}_0$ oriented along the [001], [011], and [111] crystal directions.

In this case, classical simulations are known to lead to good agreement with experiment, a consequence of the relatively large effective number of interacting neighbors n_{eff} [19,35] defined by Eq. (A3) [19]. According to Ref. [19], the values of n_{eff} for the [001], [011], and [111] crystal directions are, respectively, 4.9, 9.1, and 22.2. Given large n_{eff}, the hybrid method was also not expected to generate predictions very different from the classical ones irrespective of the choice of the quantum cluster within the method. This choice was made as follows: For each orientation of $\mathbf{B}_0$, the quantum cluster is chosen in the form of a chain extending along the crystal direction of the strongest nearest-neighbor coupling. We believe this is a reasonable approach to preserve the remaining quantum correlations. Specifically, for $\mathbf{B}_0$ along the [001] and [111] crystal directions, the cluster chains extend along the direction of $\mathbf{B}_0$; for $\mathbf{B}_0$ along the [011] direction, the chain extends along the [100] direction. The size of the simulated hybrid lattice is $9 \times 9 \times 9$ spins, which is assumed to accurately represent the hybrid lattice with an infinitely large classical part. This assumption is based on the results of Ref. [19], where no significant difference between $9 \times 9 \times 9$ and $11 \times 11 \times 11$ lattices was observed for classical simulations.

All three examples in Fig. 4 illustrate the predictive uncertainty criterion formulated earlier, namely, that, for lattices with a large number of interacting neighbors, the deviation between the predictions of the two methods quantifies the uncertainty of either of them. Indeed, hybrid and classical results diverge approximately at the same point where they start noticeably deviating from the experimental result.

A more detailed comparison of the tests for the [001], [011], and [111] directions provides further support for the role of large n_{eff}: Since n_{eff} is significantly larger for [011] and [111] than for [001], the initial agreement between the experiment and both hybrid and classical simulations extends for [011] and [111] over a longer initial time, reaching the regime of the exponential-oscillatory asymptotic behavior given by Eq. (10) (introduced in Sec. V), which, in turn, leads to the excellent overall agreement even on semilogarithmic plots. We note, however, that the statistical uncertainty of the classical and hybrid plots grows towards the end of the plotting range and, in some cases, becomes larger than the thickness of the plotted lines (see the Supplemental Material [34]). This likely explains the discrepancies between the experiment and the simulations for the [011] and [111] directions. However, for the [001] direction, the small discrepancy between the hybrid and classical simulations seen on the semilogarithmic plot is statistically significant. It leads to small differences between the parameters characterizing the long-time regime, namely, the constants of exponential decay and the oscillation frequencies. The small differences of these parameters then lead to the growing differences between classical and hybrid FIDs at longer times in Fig. 4(a). These differences, while barely visible on the linear plot, become amplified on the semilogarithmic plot [inset of Fig. 4(a)], where the classical simulations exhibit somewhat better agreement with experiment than the hybrid ones. We believe, however, that this better agreement is accidental—classical simulations in this case do not have the required predictive accuracy. In order

TABLE I. The values of γ and ω obtained from fitting the functional dependence (10) to the FIDs presented in Fig. 4(a). The fitting plots themselves can be found in the Supplemental Material [34].

	ω (rad/ms)	γ (1/ms)
Experiment	151.6	52
Hybrid	142.8	55
Classical	158.5	56

to substantiate this view, we present in Table I the values of the long-time exponential decay constants and frequencies for classical hybrid and experimental FIDs. There one can observe that both classical and hybrid calculations predict the long-time constants with an accuracy of 5%–7%, and the experimental values fall just into this range.

Beyond CaF_2, the hybrid method is supposed to be of most value in those cases where the direct quantum simulations cannot access the thermodynamic limit for the correlation functions of interest, while at the same time the effective number of interacting neighbors n_{eff} is not large enough to justify purely classical calculations, for example, three-dimensional lattices that can be divided into one-dimensional chains with stronger coupling within each chain and weaker coupling between the chains, such as fluorapatite [36], or when spins can be divided into strongly coupled pairs as in ^{13}C diamond with external magnetic field along the [111] direction [37]. The performance of the hybrid method in the above settings should be the subject of future tests.

V. DISCUSSION

Overall, Figs. 2, 3, and 4 and the additional tests in the Supplemental Material [34] illustrate that the hybrid method produces mostly very accurate predictions. As we now explain, the rare situations where the method's predictive accuracy is limited can be understood from the analysis of the asymptotic long-time behavior of $C_\alpha(t)$.

There exists substantial experimental [20,38–40] and numerical [19,32,41,42] evidence, also supported by theoretical arguments [43–45], that, despite widely varying shapes of correlation functions $C_\alpha(t)$, their long-time behavior in nonintegrable systems has the universal form

$$C_\alpha(t) \cong e^{-\gamma t} \quad \text{or} \quad C_\alpha(t) \cong e^{-\gamma t}\cos(\omega t + \phi), \tag{10}$$

where γ and ω are constants of the order of $1/\tau_c$. The asymptotic behavior(10) represents the slowest-decaying relaxational mode of the system [44]. Typically, it becomes dominant after a time of the order of several τ_c. Therefore, if one manages to accurately compute $C_\alpha(t)$ over the above initial time interval, then good overall accuracy is ensured. This is what the hybrid method achieves in a typical setting.

On the basis of the above consideration, one can anticipate that the hybrid method would predict the asymptotic time constants γ and ω with *absolute* uncertainty ϵ/τ_c, where ϵ is a number significantly smaller than 1. Yet such an uncertainty may lead to noticeable discrepancies in two problematic cases [44]: In the first, the slowest relaxational mode is characterized by $\gamma \ll 1/\tau_c$, and hence, the *relative* uncertainty of predicting γ may be large [see Fig. 2(c)]. In the second problematic case, the asymptotic behavior is characterized by an accidental competition between the two slowest relaxation modes with exponential decay constants γ_1 and γ_2 such that $|\gamma_2 - \gamma_1| \ll 1/\tau_c$. As a result, the long-time behavior can be significantly distorted in an approximate calculation. The above analysis further implies that the competition between two relaxational modes in the long-time regime is accompanied by the increased sensitivity of direct quantum simulations to the size and shape of the quantum cluster, which, in turn, prevented us from conclusively testing the hybrid method in the presence of two-mode competition (see the Supplemental Material [34]).

We finally remark that there exists a straightforward extension of the present method, where, instead of dividing the simulated lattice into a quantum cluster and a classical environment, one can divide it into computationally manageable quantum clusters coupled to each other via local fields of the form (7) obtained from the quantum-mechanical expectation values of spin operators within each cluster. Our preliminary investigations have not revealed any clear computational advantages of the latter approach in comparison with the hybrid method.

VI. CONCLUSIONS

In conclusion, we proposed a hybrid quantum-classical method of simulating high-temperature dynamics of nuclear spins in solids. The method exhibits excellent overall performance for quantum spin lattices with different dimensions and with different interactions. It comes with a long-sought internal estimate of the predictive accuracy, which was validated in each of the large number of tests we have performed. The method can therefore be used to make reliable predictions of NMR spin-spin relaxation in various materials with the goal of extracting unknown microscopic information, such as the distances between nuclei or the mechanisms of coupling between them.

ACKNOWLEDGMENTS

The authors are grateful to O. Lychkovskiy and A. Rozhkov for discussions. This work was supported by a grant from the Russian Science Foundation (Project No. 17-12-01587).

APPENDIX A: CLASSICAL SIMULATIONS

The equations of motion for classical spins are obtained from Hamiltonian (5) with the help of Poisson brackets [6] $\{s_m^\alpha, s_n^\beta\}_P = \delta_{mn}\, e_{\alpha\beta\gamma}\, s_m^\gamma$, which gives

$$\dot{\mathbf{s}}_m = \{\mathbf{s}_m, \mathcal{H}_\mathcal{C}\}_P = \mathbf{s}_m \times \left(\mathbf{h}_m^{\mathcal{CC}} + \mathbf{h}_m^{\mathcal{QC}}\right), \tag{A1}$$

where

$$\mathbf{h}_m^{\mathcal{CC}} = -\sum_{n\in\mathcal{C}} \begin{pmatrix} J_{m,n}^x s_n^x \\ J_{m,n}^y s_n^y \\ J_{m,n}^z s_n^z \end{pmatrix}. \tag{A2}$$

The infinite-temperature state is characterized by completely random orientations of classical spins. Therefore, the initial spin vectors $\{\mathbf{s}_m(0)\}$ were generated as radius vectors of points randomly sampled on a sphere of radius

$\sqrt{S(S+1)} = \sqrt{3}/2$ with uniform probability distribution. The length of classical spin vectors $\sqrt{S(S+1)}$ guarantees that the characteristic time τ_c is the same for classical and quantum lattices. It also guarantees the equality of the second moments $M_2 \equiv -C''_\alpha(0)/C_\alpha(0)$ for the two lattices. With such a choice, correlation functions corresponding to purely quantum and purely classical lattices are known to become very close to each other [10,19,46] when the effective number of interacting neighbors of each spin

$$n_{\text{eff}} \equiv \frac{\left[\sum_n \left(J_{mn}^{x2} + J_{mn}^{y2} + J_{mn}^{z2}\right)\right]^2}{\sum_n \left(J_{mn}^{x2} + J_{mn}^{y2} + J_{mn}^{z2}\right)^2} \tag{A3}$$

is greater than 4 [19]. It was also shown analytically in Ref. [35] that, in the limit of an infinite number of interacting neighbors, the two kinds of correlation functions are supposed to become identical.

APPENDIX B: QUANTUM SIMULATIONS

The dynamics of quantum clusters is simulated by the method of direct time integration of the Schrödinger equation

$$\frac{d}{dt}|\psi(t)\rangle = -i\mathcal{H}|\psi(t)\rangle \tag{B1}$$

without the complete diagonalization of the Hamiltonian [32]. In comparison with the latter, the direct integration allows one to treat larger quantum clusters numerically exactly because it does not require one to store in the computer memory either density matrices or unitary transformations, which are dense $N \times N$ matrices. Instead, only the wave function vector and the sparse Hamiltonian matrix are stored.

Each simulation starts from a randomly sampled pure quantum state (a superposition of eigenstates). These initial states are generated as

$$|\psi\rangle = \sum_{k=1}^{N} c_k |k\rangle, \tag{B2}$$

where $|k\rangle$ is a full orthonormal basis and $c_k \equiv a_k e^{i\varphi_k}$ are complex quantum amplitudes, in which φ_k are phases randomly sampled from interval $[0, 2\pi)$ and a_k are real numbers, whose squares $p_k \equiv a_k^2$ are sampled according to the probability distribution [32,47]

$$P(p_k) = N \exp(-N p_k). \tag{B3}$$

The wave functions $|\psi\rangle$ are then normalized. Thus-generated wave functions $|\psi\rangle$ are uniformly distributed over the unit hypersphere $\langle\psi|\psi\rangle = 1$ in the Hilbert space of the cluster. Such a distribution represents the infinite-temperature ensemble.

Once $|\psi(t)\rangle$ is obtained, one can compute the quantum expectation value $\langle\psi(t)|\sum_m S_m^\alpha|\psi(t)\rangle$ and then use it to obtain the correlation function $C_\alpha(t)$ (see below).

APPENDIX C: NUMERICAL INTEGRATION OF QUANTUM AND CLASSICAL EQUATIONS OF MOTION

In hybrid simulations, the dynamical equations (A1) and (B1) are integrated jointly using an explicit Runge-Kutta scheme of the fourth order with a fixed time step of $2^{-7}\, J^{-1}$ or, in some cases, $2^{-6}\, J^{-1}$ (to speed up the calculations). The time unit J^{-1} is defined as follows: for one-dimensional and two-dimensional lattices, $J = \sqrt{J_x^2 + J_y^2 + J_z^2}$, where J_x, J_y, J_z are the nearest-neighbor coupling constants; for the three-dimensional CaF_2 lattice, $J = g^2\hbar^2/a_0^3$, where g is the gyromagnetic ratio and a_0 is the cubic lattice period, both appearing in Eq. (F1) below. The choice of the time step is discussed in Refs. [19,32]. Purely classical or purely quantum simulations are performed as the appropriate limit of the hybrid simulations. The numbers of computational runs (realizations of the time evolution of the system starting from randomly chosen initial conditions) from which the plotted correlation functions were extracted are given in the Supplemental Material.

APPENDIX D: SUPPRESSION OF THE EXPECTATION VALUES OF QUANTUM OPERATORS BY THE FACTOR $1/\sqrt{N+1}$

Let us consider a cluster of N_Q spins 1/2 with the dimension of the Hilbert space $N = 2^{N_Q}$. Let us further consider quantum operator A, which has the infinite-temperature average $\langle A\rangle \equiv \frac{1}{N}\text{Tr}A = 0$ and the variance $\langle A^2\rangle \equiv \frac{1}{N}\text{Tr}A^2 \equiv A_{\text{rms}}^2$. This can be the operator of the local field or the projection of an individual spin or the operator of the total spin polarization. Here we show that, for a wave function $|\psi\rangle$ randomly sampled in the Hilbert space of the cluster according to prescription (B2),

$$\langle\psi|A|\psi\rangle \sim A_{\text{rms}}/\sqrt{N+1}. \tag{D1}$$

The intuitive explanation of this fact is based on the notion of quantum parallelism [33]. Namely, the expectation value $\langle\psi|A|\psi\rangle$ can be thought of as the average over N independent superimposed realizations of the state of the system, and as a result, a factor of the order $1/\sqrt{N}$ suppresses the statistical fluctuations of $\langle\psi|A|\psi\rangle$ with respect to the zero average.

Since the difference between $\sqrt{N}$ and $\sqrt{N+1}$ may become important for small quantum clusters, we now formally derive the factor $1/\sqrt{N+1}$ in Eq. (D1) by demonstrating that

$$\sqrt{[\langle\psi|A|\psi\rangle^2]_\psi} = A_{\text{rms}}/\sqrt{N+1}, \tag{D2}$$

where $[\cdots]_\psi$ denotes the Hilbert space average over the infinite-temperature ensemble of the pure quantum states defined by Eq. (B2). In terms of this average,

$$[\langle\psi|A|\psi\rangle]_\psi = \sum_{m,n} [c_m^* c_n]_\psi A_{mn}, \tag{D3}$$

and

$$[\langle\psi|A|\psi\rangle^2]_\psi = \sum_{k,l,m,n} [c_k^* c_l c_m^* c_n]_\psi A_{kl} A_{mn}, \tag{D4}$$

where A_{mn} are the matrix elements of A. We thus need to calculate tensors

$$F_m^k \equiv [c_k^* c_m]_\psi, \tag{D5}$$

$$D_{m,l}^{k,n} \equiv [c_k^* c_m c_n^* c_l]_\psi. \tag{D6}$$

Their form can be completely deduced from the symmetry arguments. The infinite-temperature ensemble, which we av-

erage over, is invariant with respect to the group of arbitrary unitary transformations $U(N)$ of the Hilbert space. As a consequence, tensors F_m^k and $D_{m,l}^{k,n}$ should also be invariant (transform into themselves) under the action of $U(N)$. This group contains, among other members, independent rotations of complex phases of the basis vectors and the permutations of the basis vectors.

The invariance of F_m^k with respect to the phase rotations implies that only diagonal elements F_k^k are nonzero. The invariance with respect to the permutations additionally implies that the diagonal elements should all be equal to each other. These considerations constrain the form of the tensor to

$$F_m^k = \alpha \delta_m^k, \tag{D7}$$

where α is a constant that can be found by computing the trace of F_m^k in two ways: from the definition (D5), $\sum_k F_k^k = [\sum_k |c_k|^2]_\psi = 1$, and from Eq. (D7), $\sum_k F_k^k = N\alpha$. Thus, $\alpha = 1/N$. As a result, Eqs. (D5) and (D7) give

$$[c_k^* c_m]_\psi = \frac{\delta_m^k}{N}. \tag{D8}$$

For the tensor $D_{m,l}^{k,n}$, invariance with respect to the phase rotations leaves us with nonzero elements only of the form $D_{k,n}^{k,n}$ or $D_{n,k}^{k,n}$. The symmetry of $D_{m,l}^{k,n}$ with respect to the permutations of lower indices (or upper indices) further implies that $D_{k,n}^{k,n} = D_{n,k}^{k,n}$. In terms of averaging in Eq. (D6), one should distinguish the elements $D_{k,n}^{k,n} = [|c_k|^2|c_n|^2]_\psi$ with $k \neq n$ from the elements with $k = n$, i.e., of the type $D_{k,k}^{k,k} = [|c_k|^4]_\psi$. Given the symmetry with respect to the permutations of the basis vectors, the first subset is necessarily a part of the tensor that has the form

$$D_{m,l}^{k,n} = \beta\left(\delta_m^k \delta_l^n + \delta_l^k \delta_m^n\right), \tag{D9}$$

where β is a constant. We note here that tensor (D9) is invariant with respect to all transformations belonging to the group $U(N)$ as required. It also yields the value $D_{k,k}^{k,k} = 2\beta = 2[|c_k|^2|c_n|^2]_\psi$ for the elements from the second subset. If, however, $[|c_k|^4]_\psi \neq 2[|c_k|^2|c_n|^2]_\psi$, this correction must be accounted for by adding to the right-hand side of Eq. (D9) a tensor of the form $\beta' \delta_m^k \delta_l^n \delta^{kn}$, where β' is another constant. However, a tensor defined in one basis as $\delta_m^k \delta_l^n \delta^{kn}$ does not remain invariant under all $U(N)$ transformations. Therefore, such a correction is not possible, which means that expression (D9) represents the only possible form of tensor $D_{m,l}^{k,n}$. The constant β can now be found by taking the "double trace" $\sum_k \sum_n D_{kn}^{k,n}$ in the definition (D6), which gives $\sum_k \sum_n |c_k|^2|c_n|^2 = 1$, and in Eq.(D9), where it becomes $\beta N(N+1)$. Thus, $\beta = \frac{1}{N(N+1)}$, which, together with Eqs. (D9) and (D6), implies

$$[c_k^* c_m c_n^* c_l]_\psi = \frac{\delta_m^k \delta_l^n + \delta_l^k \delta_n^m}{N(N+1)}. \tag{D10}$$

Finally, substituting Eqs. (D8) and (D10) into Eqs. (D3) and (D4), we obtain

$$[\langle\psi|A|\psi\rangle]_\psi = \frac{\mathrm{Tr}\,[A]}{N} = 0 \tag{D11}$$

and

$$[\langle\psi|A|\psi\rangle^2]_\psi = \frac{\mathrm{Tr}\,[A^2]}{N(N+1)} + \frac{\mathrm{Tr}^2\,[A]}{N(N+1)} = \frac{A_{\mathrm{rms}}^2}{N+1}, \tag{D12}$$

which gives Eq.(D2).

Now we apply the above general result to the operator of the local magnetic field of a quantum spin lattice

$$\mathbf{h}_i = -\sum_{j\neq i} \begin{pmatrix} J_{ij}^x S_j^x \\ J_{ij}^y S_j^y \\ J_{ij}^z S_j^z \end{pmatrix}. \tag{D13}$$

The rms value of $\mathbf{h}_i$ is defined as

$$h_{\mathrm{rms}} \equiv \sqrt{\frac{1}{N}\sum_{j\neq i,\alpha} \left(J_{ij}^{\alpha 2}\,\mathrm{Tr}\left[S_j^{\alpha 2}\right]\right)}. \tag{D14}$$

(The characteristic time of lattice dynamics τ_c given in the main text is obtained as $1/h_{\mathrm{rms}}$.)

If we consider the quantum expectation value $\langle\psi|\mathbf{h}_i|\psi\rangle$ for a random quantum state, then its rms value is

$$\begin{aligned} \|\langle\psi|\mathbf{h}_i|\psi\rangle\|_{\mathrm{rms}} &= \sqrt{[\langle\psi|\mathbf{h}_i|\psi\rangle^2]_\psi} \\ &= \sqrt{\sum_{j\neq i,l\neq i,\alpha} J_{ij}^\alpha J_{il}^\alpha \left[S_j^\alpha S_l^\alpha\right]_\psi}. \end{aligned} \tag{D15}$$

Using Eqs. (D11) and the fact that $[S_j^\alpha S_l^\alpha]_\psi = 0$ for $j \neq l$, we obtain

$$\|\langle\psi|\mathbf{h}_i|\psi\rangle\|_{\mathrm{rms}} = \sqrt{\sum_{j\neq i,\alpha} J_{ij}^{\alpha 2} \frac{\mathrm{Tr}\left[S_j^{\alpha 2}\right]}{N(N+1)}} = \frac{h_{\mathrm{rms}}}{\sqrt{N+1}}. \tag{D16}$$

We finally remark that the considerations of this appendix imply that the hybrid dynamics defined in Sec. III with the quantum cluster consisting of one spin 1/2 surrounded by classical spins and with the exact prefactor $\sqrt{N+1}$ in Eq. (7) instead of the approximate $\sqrt{N}$ is exactly equivalent to the purely classical dynamics of the same lattice.

APPENDIX E: REPRESENTATIONS OF CORRELATION FUNCTIONS

For purely classical systems, we extracted equilibrium correlation functions $C_\alpha(t)$ from the equilibrium noise of the quantity of interest $M_\alpha(t) = \sum_m s_m^\alpha(t)$ using the following definition:

$$C_\alpha(t) = \mathcal{N}\left[\frac{1}{T_{\max}}\int_0^{T_{\max}} d\tau\, M_\alpha(\tau+t) M_\alpha(\tau)\right]_{i.c.}, \tag{E1}$$

where $\mathcal{N}$ is a normalization constant and $[\cdots]_{i.c.}$ denotes averaging over the infinite-temperature ensemble of initial conditions. The time $T_{\max}$ was chosen to be sufficiently large ($T_{\max} \gg \tau_c$, $T_{\max} \gg t$). In principle, if the system is ergodic and the limit $T_{\max} \to \infty$ is taken, then the averaging over the initial conditions is not necessary. In practice, however, given the unclear ergodization timescales, we perform the additional averaging over the initial conditions both as a consistency

check and as a way to improve the efficiency of the averaging procedure.

For purely quantum systems, the correlation function of interest is, at first sight, defined differently, namely, $C_\alpha(t) \simeq \mathrm{Tr}\{e^{i\mathcal{H}_\mathcal{Q}t} M_\alpha e^{-i\mathcal{H}_\mathcal{Q}t} M_\alpha\}$, where $M_\alpha = \sum_m S_m^\alpha$ is a quantum-mechanical operator. It was, however, proven in Ref. [32] that one can obtain the result of the above quantum trace calculation with the help of formula (E1), where classical projections $M_\alpha(t)$ are replaced by quantum-mechanical expectation values $M_\alpha(t) = \langle\psi(t)|\sum_{m\in\mathcal{Q}} S_m^\alpha|\psi(t)\rangle$ associated with the time evolution of a randomly chosen wave function (B2). The amplitude of the resulting quantum noise of $M_\alpha(t)$ is, however, smaller than that of the classical counterpart by the factor $1/\sqrt{N}$.

At the level of the basic idea, our method of hybrid simulations compensates the above amplitude mismatch by redefining $M_\alpha(t)$ with the help of Eq. (8) and then obtaining $C_\alpha(t)$ using Eq. (E1) with the newly defined $M_\alpha(t)$. However, in the final application of the method, we introduce an additional technical modification aimed at reducing the effect of the quantum-classical border. Namely, we use the fact that, due to the translational invariance of the original quantum problem, the correlation function of interest can be reexpressed as $C_\alpha(t) \simeq \mathrm{Tr}\{e^{i\mathcal{H}_\mathcal{Q}t} M_\alpha e^{-i\mathcal{H}_\mathcal{Q}t} S_m^\alpha\}$, where S_m^α is the αth projection operator of any spin on the lattice. Moreover, S_m^α in this expression can be further replaced by the sum $M'_\alpha = \sum_{m\in\mathcal{Q}'} S_m^\alpha$ over any subset $\mathcal{Q}'$ of spins on the lattice, which, therefore, we can choose at our discretion. The presence of the quantum-classical border in the hybrid simulations breaks the translational invariance of the system, thereby making different choices of M'_α nonequivalent from the viewpoint of the approximation error. We minimize this error by choosing subset $\mathcal{Q}'$ to consist of one or several equivalent quantum spins which are farthest from the quantum-classical border.

Finally, we combine all the above relations to arrive at the expression for the correlation function actually used in our hybrid simulations:

$$C_\alpha(t) = \mathcal{N}\left[\frac{1}{T_{\max}}\int_0^{T_{\max}} d\tau\, M_\alpha(\tau+t) M'_\alpha(\tau)\right]_{i.c.}, \qquad \text{(E2)}$$

where $M_\alpha(t)$ is given by Eq. (8) and $M'_\alpha = \sqrt{N}\langle\psi(t)|\sum_{m\in\mathcal{Q}'} S_m^\alpha|\psi(t)\rangle$. For each set of initial conditions, we integrated the dynamical equations (A1) and (B1) up to time $T_{\max} \sim 10T_0$, where T_0 is the maximum time t in Eq. (E2) for which the correlation function $C_\alpha(t)$ was to be computed. The number of initial conditions was then chosen to be sufficiently large to make the resulting statistical uncertainty of $C_\alpha(t)$ negligible on the scale of the resulting plots.

We tested hybrid simulations for one- and two-dimensional lattices by comparing hybrid results with purely quantum simulations of larger spin-1/2 clusters, for which the direct integration of the Schrödinger equation could be implemented numerically (typically, up to 25 spins 1/2). For this, we used yet another representation of the correlation function [17,32]:

$$C_\alpha(t) = \mathcal{N}\left[\langle\psi(t)|\sum_m S_m|\psi_{aux}(t)\rangle\right]_{i.c.}, \qquad \text{(E3)}$$

where $|\psi(t)\rangle$ is obtained via direct integration starting from a randomly selected $|\psi(0)\rangle$, while $|\psi_{aux}(t)\rangle$ is obtained via the direct integration of the unnormalized auxiliary initial wave function $\sum_m S_m|\psi(0)\rangle$. Such a method is more efficient than the one involving formula (E2) because, for larger clusters, it requires the direct integration of only two wave functions over time T_0 (much less than $T_{\max}$) to obtain $C_\alpha(t)$ with accuracy $1/\sqrt{N}$. So far, however, we are not able to incorporate this method into a hybrid simulation scheme.

APPENDIX F: FREE INDUCTION DECAY IN CaF_2

The FID experiments in solids measure the relaxation of the total nuclear magnetization transverse to a strong magnetic field $\mathbf{B}_0$. The relaxation is caused by the magnetic dipolar interaction between nuclear spins averaged over the fast Larmor precession induced by $\mathbf{B}_0$. The effective interaction Hamiltonian in the Larmor rotating reference frame has the form (1) with coupling constants

$$J^z_{i,j} = -2J^x_{i,j} = -2J^y_{i,j} = \frac{g^2\hbar^2(1-3\cos^2\theta_{ij})}{|\mathbf{r}_{ij}|^3}, \qquad \text{(F1)}$$

where the z axis is chosen along the direction of $\mathbf{B}_0$, $\mathbf{r}_{ij}$ is the vector connecting lattice sites i and j, θ_{ij} is the angle between $\mathbf{r}_{ij}$ and $\mathbf{B}_0$, and g is the gyromagnetic ratio of the nuclei. The measured FID signal is proportional to $C_x(t)$ given by Eq. (2).

In CaF_2, the ^{19}F nuclei form a cubic lattice with period $a_0 = 2.72$ Å. Their gyromagnetic ratio is $g = 2.51662 \times 10^8$ rad s^{-1} T^{-1}.

[1] I. J. Lowe and R. E. Norberg, Phys. Rev. **107**, 46 (1957).
[2] A. Abragam, *Principles of Nuclear Magnetism* (Oxford University Press, Oxford, 1961).
[3] F. Bloch, Phys. Rev. **70**, 460 (1946).
[4] B. V. Fine, T. A. Elsayed, C. M. Kropf, and A. S. de Wijn, Phys. Rev. E **89**, 012923 (2014).
[5] A. S. de Wijn, B. Hess, and B. V. Fine, Phys. Rev. Lett. **109**, 034101 (2012).
[6] A. S. de Wijn, B. Hess, and B. V. Fine, J. Phys. A **46**, 254012 (2013).
[7] J. H. Van Vleck, Phys. Rev. **74**, 1168 (1948).
[8] J. A. Tjon, Phys. Rev. **143**, 259 (1966).
[9] G. W. Parker and F. Lado, Phys. Rev. B **8**, 3081 (1973).
[10] S. J. K. Jensen and O. Platz, Phys. Rev. B **7**, 31 (1973).
[11] M. Engelsberg and N.-C. Chao, Phys. Rev. B **12**, 5043 (1975).
[12] K. W. Becker, T. Plefka, and G. Sauermann, J. Phys. C **9**, 4041 (1976).
[13] R. N. Shakhmuratov, J. Phys.: Condens. Matter **3**, 8683 (1991).
[14] A. A. Lundin, Zh. Eksp. Teor. Fiz. **102**, 352 (1992) [Sov. Phys. JETP **75**, 187 (1992)].
[15] J. Jensen, Phys. Rev. B **52**, 9611 (1995).

[16] B. V. Fine, Phys. Rev. Lett. **79**, 4673 (1997).
[17] W. Zhang, N. Konstantinidis, K. A. Al-Hassanieh, and V. V. Dobrovitski, J. Phys. Condens. Matter **19**, 083202 (2007).
[18] D. V. Savostyanov, S. V. Dolgov, J. M. Werner, and I. Kuprov, Phys. Rev. B **90**, 085139 (2014).
[19] T. A. Elsayed and B. V. Fine, Phys. Rev. B **91**, 094424 (2015).
[20] M. Engelsberg and I. J. Lowe, Phys. Rev. B **10**, 822 (1974).
[21] W. A. Coish and D. Loss, Phys. Rev. B **72**, 125337 (2005).
[22] K. A. Al-Hassanieh, V. V. Dobrovitski, E. Dagotto, and B. N. Harmon, Phys. Rev. Lett. **97**, 037204 (2006).
[23] R.-B. Liu, W. Yao, and L. J. Sham, New J. Phys. **9**, 226 (2007).
[24] P. L. Stanwix, L. M. Pham, J. R. Maze, D. Le Sage, T. K. Yeung, P. Cappellaro, P. R. Hemmer, A. Yacoby, M. D. Lukin, and R. L. Walsworth, Phys. Rev. B **82**, 201201 (2010).
[25] W. Yang, W.-L. Ma, and R.-B. Liu, Rep. Prog. Phys. **80**, 016001 (2017).
[26] E. Balcar and S. W. Lovesey, *Theory of Magnetic Neutron and Photon Scattering* (Clarendon, Oxford, 1989).
[27] A. Hams and H. De Raedt, Phys. Rev. E **62**, 4365 (2000).
[28] J. Gemmer, M. Michel, and G. Mahler, *Quantum Thermodynamics* (Springer, Berlin, 2004).
[29] S. Goldstein, J. L. Lebowitz, R. Tumulka, and N. Zanghì, Phys. Rev. Lett. **96**, 050403 (2006).
[30] S. Popescu, A. J. Short, and A. Winter, Nat. Phys. **2**, 754 (2006).
[31] C. Bartsch and J. Gemmer, Phys. Rev. Lett. **102**, 110403 (2009).
[32] T. A. Elsayed and B. V. Fine, Phys. Rev. Lett. **110**, 070404 (2013).
[33] G. A. Álvarez, E. P. Danieli, P. R. Levstein, and H. M. Pastawski, Phys. Rev. Lett. **101**, 120503 (2008).
[34] See Supplemental Material at http://link.aps.org/supplemental/10.1103/PhysRevB.98.214421 for (i) finite-size analysis for quantum clusters used in Figs. 2 and 3; (ii) additional tests of the hybrid method; (iii) statistical errors for the semilogarithmic plots in the insets of Fig. 4; (iv) long-time fits for the inset in Fig. 4(a); and (v) statistics behind the plots.
[35] A. A. Lundin and V. E. Zobov, J. Magn. Reson. **26**, 229 (1977).
[36] M. Engelsberg, I. J. Lowe, and J. L. Carolan, Phys. Rev. B **7**, 924 (1973).
[37] K. Lefmann, B. Buras, E. J. Pedersen, E. S. Shabanova, P. A. Thorsen, F. Berg Rasmussen, and J. P. F. Sellschop, Phys. Rev. B **50**, 15623 (1994).
[38] S. W. Morgan, B. V. Fine, and B. Saam, Phys. Rev. Lett. **101**, 067601 (2008).
[39] E. G. Sorte, B. V. Fine, and B. Saam, Phys. Rev. B **83**, 064302 (2011).
[40] B. Meier, J. Kohlrautz, and J. Haase, Phys. Rev. Lett. **108**, 177602 (2012).
[41] K. Fabricius, U. Löw, and J. Stolze, Phys. Rev. B **55**, 5833 (1997).
[42] B. V. Fine, J. Stat. Phys. **112**, 319 (2003).
[43] P. Borckmans and D. Walgraef, Phys. Rev. **167**, 282 (1968).
[44] B. V. Fine, Int. J. Mod. Phys. B **18**, 1119 (2004).
[45] B. V. Fine, Phys. Rev. Lett. **94**, 247601 (2005).
[46] C. Tang and J. S. Waugh, Phys. Rev. B **45**, 748 (1992).
[47] B. V. Fine, Phys. Rev. E **80**, 051130 (2009).